Mapping Feeding-Strike Related Functional Morphology Across Syngnathoidei

Alexander DuToit[1,6], Graham Short[2,3,4], Cassandra Donatelli[5],
Karly Cohen[6], Roi Holzman[6,7,8]

Reu Blinks Research Fellowship 2025
Summer 2025

[1]University of Massachusetts Amherst
[2]California Academy of Sciences
[3]Australian Museum
[4]Burke Museum
[5]University of Washington Tacoma
[6]University of Washington Friday Harbor Laboratories
[7]Tel Aviv University
[8]Steinhardt Museum

Contact Information:
Alexander DuToit
Department of Biology
University of Massachusetts Amherst
Morrill Science Center, 80 Campus Center Way,
Amherst, MA 01003
adutoit@umass.edu

Keywords: Syngnathiformes, Syngnathiodei, Syngnathidae, Seahorses, Pipefish, functional morphology, CT scanning, suction feeding

Abstract

Syngnathoidei, a diverse suborder of syngnathiform fish, include the families Aulostomidae and Fistularidae (cornetfish and trumpetfish), Centriscidae (snipefish and shrimpfish), Solenostomidae (ghost pipefish), and Syngnathidae (seahorses, pipefish, and seadragons). These specialized suction feeders are capable of capturing small zooplankton with remarkable speed. These rapid feeding strikes are powered by elastic energy stored in the epaxial tendons, which is released during prey capture. In seahorses (genus *Hippocampus*), this system is further enhanced by an elongated sternohyoideus tendon, creating a secondary spring that supplements the epaxial system. The effect of this increasing functional complexity on the wider mechanical linkage system remains unclear in this morphologically diverse clade. Here, we used μCT scan data to measure functionally relevant bone lengths across 30 syngnathiform species from 5 families. We then compared those lengths across a phylogeny to determine where certain features involved in the suction feeding system evolved. We found significant correlations between various functional measurements and identified a robust phylogenetic signal for urohyal length. This marks a transition from a one to two-spring system between pipefish and seahorses, as an elongated sternohyoideus tendon replaces the shortened urohyal bone. We also report ossification of the epaxial tendon in several closely related pipefishes, a feature that may constrain their ability to generate high-powered feeding strikes relative to other lineages.

Introduction

Suction feeding is a ubiquitous method of prey capture across many fish families (Olsen et al. 2022). Suction feeding relies on the generation of low pressure inside the buccal cavity, leading to flow that draws prey into the mouth (Day et al., 2015; Muller et al., 1982). To generate this low pressure, the entire buccal cavity is expanded by a combination of a forward protrusion of the premaxilla, adduction of the suspensoria (a combination of bones creating both sides of the buccal cavity), elevation of the neurocranium, and depression of the hyoid.

The ability to suction feed relies on adequate power being generated to expand the buccal cavity and create an inflow of water. Typically, fish use a combination of axial and cranial muscles to generate this power, with the axial muscles providing most of the power needed for this feeding stratagem (Camp et al., 2015; Camp et al., 2018; Carroll and Wainwright, 2006). The primary muscles used are the epaxial muscles dorsally, and the sternohyoideus and hypaxial muscles ventrally. The power output of these muscles largely determines the magnitude of suction generated for feeding (Carrol et al. 2004; Camp et al. 2015).

One method of suction feeding, so-called ‘pivot-feeding,’ allows some members of Syngnathoidei (seahorse, pipefish, snipefish, etc.) to achieve remarkably high-power output while simultaneously rotating their heads upwards to bring prey nearer to their mouths. This high-power output is attributed to elastic tendons, which store energy, driving feeding strikes multiple times more powerful than achievable by musculature alone (Roos et al., 2009; Van Wassenbergh and Aerts, 2008; Van Wassenbergh et al., 2014; Adivan et al., 2023). This biomechanical mechanism that transmits power and

motion for the pivot feeding, when projected onto a 2D plane, can roughly be described as a four-bar linkage. A 4 bar linkage is a 2-dimensional model in which 4 bars of various lengths are joined at their ends with pivots and then may move in space. The curves that they trace are constrained by the specific lengths of the constituent parts (Muller et al., 1987). In this model, hyoid apparatus, neurocranium-suspensorium linkage, pectoral girdle linkage, and urohyal-sternohyoideus link make up the bars (going in a clockwise direction starting from the leftmost bar). There are limitations to this simplification. A 5th joint between the Hyomandibular and neurocranium acts primarily in a lateral direction and so is not considered in this projection. Additionally, the link made from the urohyal bone and sternohyoideus tendon can change length depending on muscular contraction (Figure 1). Varying the relative lengths of the bars can produce markedly different properties, such as increased magnitude or initial rate of neurocranial elevation (Muller et al., 1987; Longo et al., 2018).

The epaxial tendons, which store elastic energy to power feeding strikes, connect to the supraoccipital bone near its anterior tip, forming a spring that powers a quasi-four-bar linkage (Roos et al., 2009). The storage of elastic energy can be described as a latch-mediated spring-actuated system (LaMSA). A LaMSA system involves the storage of elastic or other energy, the release of which is regulated by a latching mechanism. In seahorses, pipefish, and other Syngnathiformes, elastic energy is stored in the epaxial tendons, counterbalanced by the force applied by the sternohyoideus muscles (Divi et al., 2020; Longo et al., 2019; Longo et al., 2018; Van Wassenbergh et al. 2013; Van Wassenbergh et al., 2008).

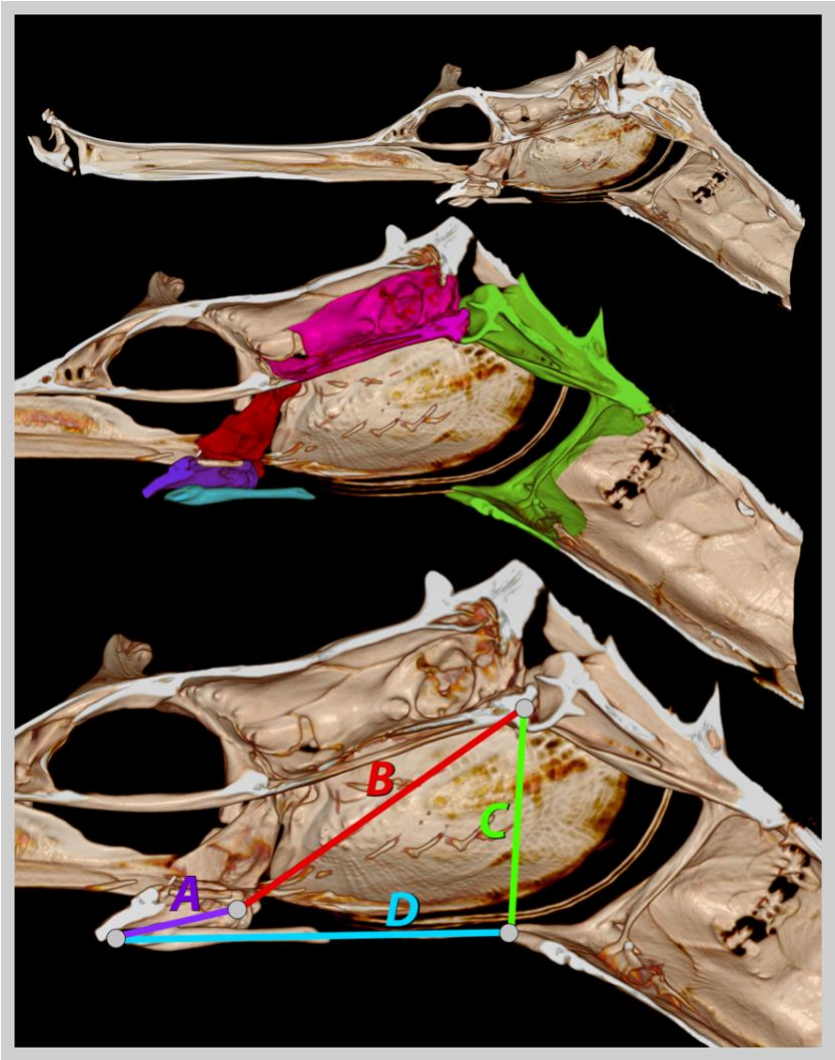

Figure 1.
Top) CT scan model of *Haliichthys taeniophorus* cut dorsoventrally. Middle) Color-coded regions of bones. hyoid is purple, Hyomandibular is red, Neurocranial linkage is pink, Pectoral Girdle linkage is green, and urohyal is blue. Bottom) Approximation of the feeding-strike mechanism as a 4-bar linkage. A is the urohyal link, B is the suspensoria-neurocranial link, C is the Pectoral Girdle link, and D is the urohyal-sternohyoideus tendon link.

The interaction of the hyoid and urohyal-sternohyoideus tendon linkage constitutes an overlocking mechanism: the 'Latch' of the system, in which tension in the sternohyoideus tendon and urohyal (which act in line), keep the hyoid raised against bony internal mouth plates (Longo et al., 2018; Leysen et al., 2011). While the system is latched, the epaxial muscles exert force on the epaxial tendons, resulting in their tensioning and the storage of elastic energy. The tension from the epaxial tendon creates

a torque around the joint between the vertebral column and the neurocranium, which is balanced by the torque imparted by the sternohyoideus muscle, sternohyoideus tendon, and urohyal through the hyoid. In this configuration, the hyoid is in line, or slightly raised, against internal bony mouth plates. While in this position, it can balance the torque from the epaxials by applying an opposite torque at the joint of the Hyomandibular and hyoid.

The mechanism may be triggered by small muscles, such as the activation of the protractor hyoidei or the relaxation of the adductor arcus palatini (Van Wassenbergh et al., 2008; Leysen et al., 2011; Muller, 1987). This triggering event causes the hyoid to change from its stable overlocked configuration to an unstable configuration in which the hyoid is retroverted downwards, pulled by the urohyal, sternohyoideus tendon, and sternohyoideus muscle. Once the hyoid has departed from its locked configuration, the sternohyoideus muscles no longer provide a toque opposing that of the epaxials. The Epaxial tendons are now able to release their stored energy and elevate the neurocranium. This has the combined effect of swinging the snout upwards towards prey while expanding the buccal cavity downward with the movement of the hyoid (Van Wassenbergh et al., 2008; Muller, 1987, Longo et al., 2018; Van Wassenbergh et al., 2013).

A notable difference between seahorses and most pipefish is the length of the urohyal bone. In seahorses, this bone is much reduced, and the sternohyoideus tendon (which attaches to its posterior) is elongated (Leysen et al., 2011). The elongated sternohyoideus tendon can act as a second spring in seahorses, powering the retroversion of the hyoid. This second energy storage source aids in the rapid elevation of the

neurocranium and expansion of the buccal cavity (Van Wassenbergh et al., 2013; Van Wassenbergh et al., 2014; Avidan et al., 2023).

Examining functional morphology allows us to gain insight into the systems that drive complex movements. Rather than focusing only on the direct results of biological dynamic systems, a morphological approach can shed light on how a system actually works. Morphological studies in fish feeding often focus on how performance is affected by certain traits. For example, Carroll et al. (2004) used the buccal cavity volume as a predictor of buccal pressure in feeding and feeding style. Avidan et al. (2023) used measurements of tendons in seahorses as a predictor of power output, and acceleration of water and the head. Others like Leysen et al. (2011) use detailed morphological descriptions of both bone and soft tissue to inform theory on the roles of different elements in the complex system of seahorse and pipefish feeding strikes.

Here, we aim to shed light on the evolution of functional traits relating to suction feeding across Syngnathoidei. We collected measurements using microCT scanning. To view trends across the suborder, we compare features such as urohyal length, hyoid length, and lever ratios across a resolved phylogeny. In examining these we uncover significant phylogenetic signals for traits such as urohyal bifurcation and epaxial tendon ossification that have the potential to limit the elastic energy storage system. To examine how gross functional morphology related to suction feeding changed evolutionarily, we conducted PCAs of all functional traits measured, inquiring whether groups converged or stayed morphologically distinct based on their ancestry. We then take a more granular focus on the role of the 4 bar linkage system in relation to other functional measurements. The lengths constituting the 4 bar linkage should be of central importance to the entire

functional system. To test this, we performed RDAs on urohyal length and all four of the linkage lengths to assess their impact on the functional system as a whole.

Methods

Specimen selection and scanning

We obtained Computed Tomography (CT) scans of species from ancestral clades at 25 MYA as reported by Stiller et al. 2022. Specimens were scanned at The University of Washington, Friday Harbor Labs Karel F. Liem Bioimaging Facility, or downloaded from MoprhoSource.org. We used one specimen for each species in our sample. We obtained scans of 32 species but did not use 2 in our analysis: *Aulostomus chinensis*, *Bhanotia fasciolata, Campichthys galei, Centriscus scutatus , Choeroichthys brachysoma*, *Cosmocampus albirostris, Dunckerocampus baldwini, Festucalex erythraeus, Fistularia commersonii*, *Halicampus grayi, Halicampus mataafae*, *Halicampus punctatus, Haliichthys taeniophorus, Hippichthys penicillus, Hippocampus bargibanti, Hippocampus colemani, Hippocampus erectus, Hippocampus histrix, Hippocampus kuda, Hippocampus minotaur, Hippocampus pontohi, Idiotropiscis lumnitzeri, Macroramphosus scolopax, Microphis deocata, Minyichthys myersi, Nerophis ophidion, Siokunichthys nigrolineatus, Solenostomus cyanopterus, Stigmatopora nigra, Syngnathus californiensis, Syngnathus typhle,* and *Urocampus carinirostris*. Scans were either taken of specimens' heads or whole bodies, at resolutions between 4µm and 71.1µm voxel size, with voltages ranging from 50kV to 130kV and amperages from 64µA to 200µA (Appendix Tables 1a-1b). *Hippocampus minotaur* and *Campichthys galei* were excluded from the analysis due to their unclear phylogenetic relationship.

Hippocampus colemani was not present on the phylogeny from Stiller et al. 2022, and was replaced by their closest relative (*Hippocampus denise*), which was present in the phylogeny.

CT Scan Landmarking

We used 3D Slicer (Fedorov et al., 2012; 3D Slicer) with modules SlicerMorph (Rolfe et al., 2021) to visualize all scans, as well as place landmarks. Landmarks' coordinates were reported in global Cartesian coordinates in millimeters. 36 Landmarks were chosen, representing points of importance in the LaMSA and power amplification system, as well as points related to general cranial morphology (Van Wassenbergh et al., 2013; Longo et al., 2018; Roos et al., 2009). Points such as those determining the spacing of the Supraoccipital and Anterior Nuchal Plate were measured as possible diagnostic characters (Short and Trnski, 2021). For points that did not exist on some species (such as the nuchal plates), a coordinate of (0,0,0) at the origin was used as a placeholder. No points that exist were located at (0,0,0). Figure 2 illustrates the landmarks as placed on Minyichthys myersi.

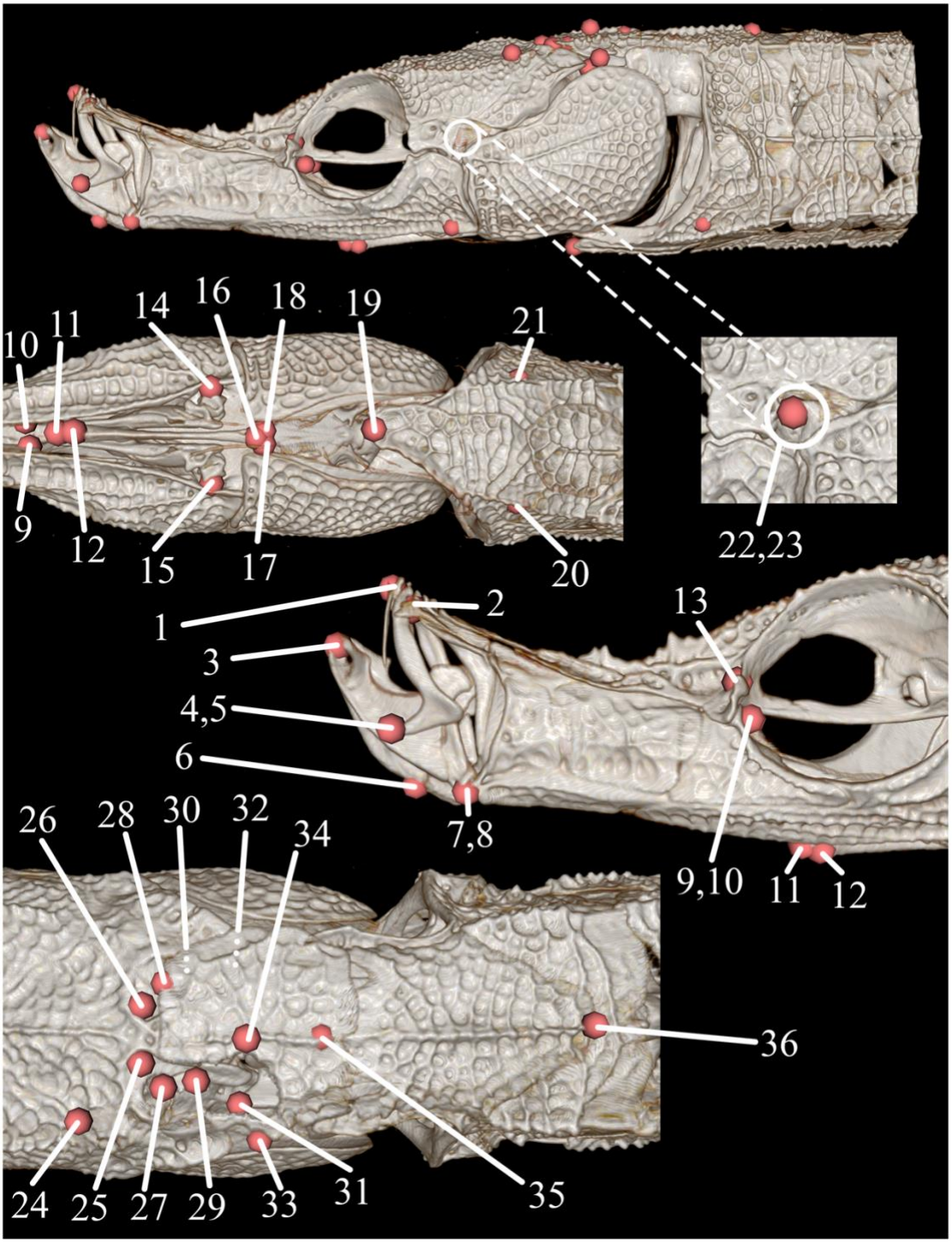

Figure 2. Landmarks placed on Minyichthys myersi in the same positions as are placed in all species sampled from Syngnathoidei. Points with two numbers listed are

symmetric on both left and right. (1) Symphysis of premaxilla (2) Tip of vomeral bone. (3) Tip of dentary (4,5) Anterior projection of premaxilla (6) Lowest point of the dentary (7,8) angular-quadrate Joint (9,10) Protrusion of interopercular bone (11) Anterior of the symphysis of ceratohyals (12) Anterior of urohyal (13) Anterior of left orbit (14,15) Joint of the hyomandibular and hyoid (16) Split of urohyal (17,18) Posterior protrusion of urohyal (19) Anterior ventral projection of pectoral girdle (20,21) Pectoral girdle at max width (22,23) Neurocranial-hyomandibular joint, shown in cutaway (24) Left base of supraoccipital (25,26) Anterior attachment of epaxial tendons (27,28) Anterior of epaxial tendon ossification (29,30) Posterior of epaxial tendon ossification, left shown in cutaway (31,32) Anterior projection of the first vertebrae, left show in cutaway (33) Left base of anterior nuchal plate (34) distal tip of anterior nuchal plate (35) Anterior of posterior nuchal plate (36) Posterior of posterior nuchal plate

Analysis

We created 4 points as averages of symmetric points that occur on both sides of the head, and used these as analogs of a 2-dimensional 4-bar linkage plus an upper lever arm projected onto the sagittal plane. The artificially created points were the midpoint of the hyoid joints, the midpoint of the suspensoria (Hyomandibular)-neurocranium joint, the midpoint of the anterior vertebral protrusions (the top joint of the linkage), and the midpoint of the epaxial tendon connection to the supraoccipital (the midpoint of the top of the lever arm). Sagittally projected lengths are those created from one or more of these points.

We calculated Euclidean distances between all landmarks in R (R Core Team 2025). We then selected a subset of mechanically relevant lengths. To correct for size, we

divided every length measurement by the Fixed Link: the length between the joint of the neurocranium and the first vertebrae, and the bottom of the pectoral girdle.

We calculated the kinematic transmission (KT) coefficient to relate the depression of the hyoid to the elevation of the neurocranium. KT is the ratio of the output angle (Neurocranial elevation) to input angle (between hyoid and urohyal). An angle of 50º was used as the input for this calculation.

We examined urohyal length, urohyal bifurcation, snout length, lever ratio (Fixed Link/Top Lever), KT, epaxial ossification, and sagittally projected hyoid length, and plotted these on a phylogeny (Stiller et al., 2022). We computed Pagel's lambda for these measurements and performed 2-tailed tests for significance with R package phytools (Revell 2024).

We performed a PCA with package FactoMineR (Lê et al., 2008) of these lengths across all study species. We also performed a PCA for only the family Syngnathidae to exclude morphological outliers. We used the R package phytools to create a phylomorphospace from the PCA and phylogeny (Revell 2024).

We performed 2 sets of RDAs with the R package vegan (Oksanen et al., 2025). The first two RDAs used urohyal length as an explanatory variable for the other functional lengths. One RDA was on Synganthoidei (Syngnathoidei includes Syngnathidae) and the other on Syngnathidae`. The second set of RDAs used 4 bar linkages: urohyal length, projected fixed link, projected neurocranium-suspensoria link, and projected hyoid Link, as explanatory variables for the remaining lengths. Again, these were performed both over Synganthoidei and Syngnathidae.

Results

Point and Length Measurements

We measured 36 point landmarks on 30 species (Figure 3). From these, we calculated lengths in mm between all points, and chose lengths relevant to energy storage and feeding strikes (Appendix Tables 2a-2b).

Figure 3. Cross sections of all sampled members of Syngnathoidei rendered from CT scans.

Lengths vary widely between species. Standardizing length by the 'fixed link' of the 4-bar linkage (Muller, 1987) allows us to compare relative lengths across species. Figures 4-10 show how urohyal length, snout length, lever ratio (Fixed Link/Top Lever), KT, epaxial ossification, Sagittally projected hyoid length, and urohyal split, occurring when the urohyal bifurcates to follow each side of the sternohyoideus tendons and muscles, vary across the known phylogeny. Pagel's Lambda and associated p-value based on a two-tailed test for the phylogenetic signal of these traits yielded a strong phylogenetic signal for all traits tested except for lever ratio, intrafamily KT and intrafamily hyoid length. KT and hyoid length still had significant phylogenetic signals over the suborder Syngnathoidei. These results are summarized in Table 4.

Table 4.

Pagel's lambda and associated p values for urohyal length, snout length, lever ratio (Fixed Link/Top Lever), KT, epaxial ossification, sagittally projected hyoid length, and urohyal split. Significant values are bolded.

	Urohyal Length	**Snout Length**	Lever Ratio	KT	Epaxial ossification	Hyoid Length	**Urohyal Split**
Syngnathoidei Pagel's λ	**0.999927**	**0.999927**	7.33 x 10^{-5}	**0.755**	**0.999927**	**0.871981**	**0.999927**
Syngnathoidei p value (two tailed)	**1.86 x 10^{-5}**	**8.56 x 10^{-5}**	1	**0.036**	**3.51 x 10^{-5}**	**0.0057**	**0.0014**
Synagnthidae Pagel's λ	**0.999927**	**0.999927**	7.33 x 10^{-5}	0.461018	**0.999927**	7.33x10^{-5}	**0.999927**
Synagnthidae p value (two tailed)	**1.84 x 10^{-3}**	**0.0181471**	1	0.0673	**7.8 x 10^{-3}**	1	**0.0012**

Urohyal length shows significant changes across the suborder. (Figure 4) Seahorses have notably shorter urohyals than pipefish. Within seahorses, the distinction between pygmy seahorses and non-pygmy seahorses can be seen simply from urohyal length. The bifurcation of the urohyal (Figure 5) is also highly variable across the suborder. However, seahorses are devoid of a bifurcated urohyal, as are many of their closer relatives. When a bifurcation occurs, it typically begins before the anterior protrusion of the pectoral girdle around the middle of the operculum as viewed ventrally. Lever ratio (Figure 7) does not have a significant phylogenetic signal inside the family Syngnathidae, though it does over the entire suborder. Similarly, KT (Figure 8) only has a significant phylogenetic signal when all species we sampled from the suborder Syngnthoidei are taken into consideration. Epaxial ossification has a strong phylogenetic signal. This can be seen when the level of ossification of the epaxial tendons is compared phylogenetically in Figure 9. Seahorses are devoid of epaxial ossification, many pipefish have low levels, and certain pipefish clades, as well as trumpetfish and cornetfish, have remarkably long ossification of their epaxial tendons. Hyoid length (Figure 10) is also variable, though the phylogenetic signal is only significant over the suborder. Species like *Syngnathus typhle* have elongate hyoid bones when compared to pygmy seahorses like *Hippocampus bargibanti*.

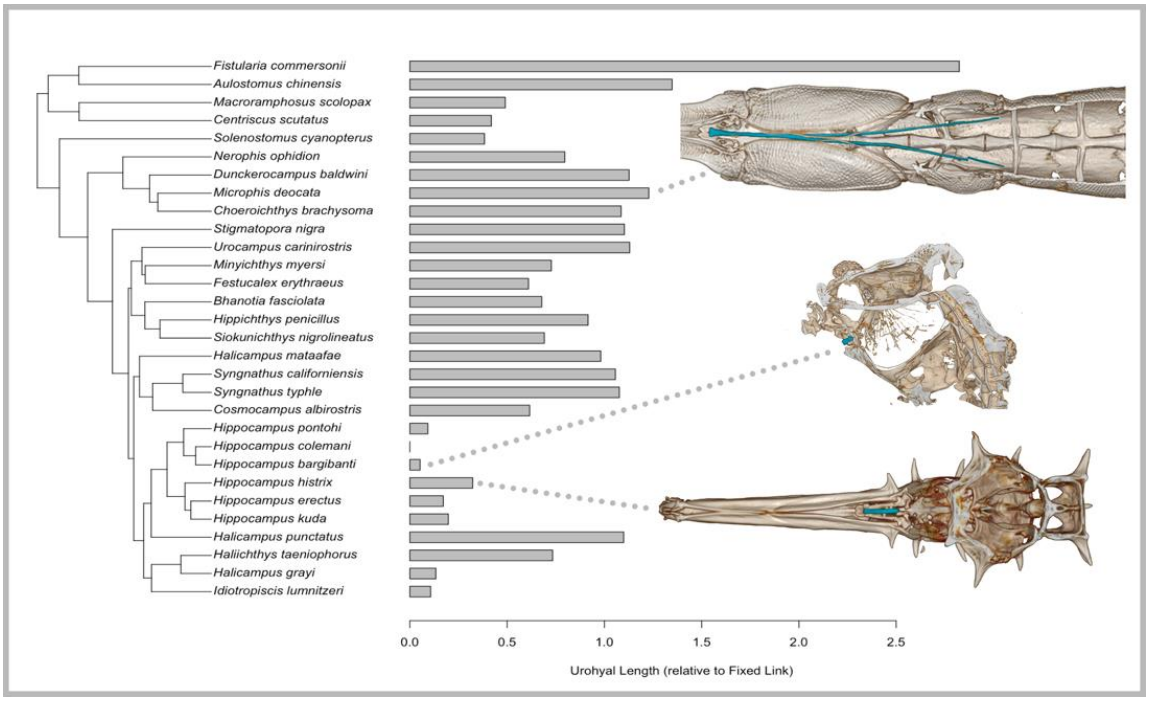

Figure 4. Phylogeny of species sampled from Syngnathoidei with urohyal bone length relative to the length of the pectoral girdle (Fixed link in the 4-bar linkage). *Hippocampus* (Seahorses) have relatively short urohyals (under 1 time hyoid length), with pygmy seahorses (*Hippocampus pontohi* and *Hippocampus bargibanti* in this sample) having the shortest. *Idiotropiscis lumnitzeri* and *Halicampus grayi* also have short uroyal bones; however, *Halicampus punctatus* and *Haliichthys taeniophorus*, have relatively long urohyals. urohyal length has a significant phylogenetic signal across the family and suborder.

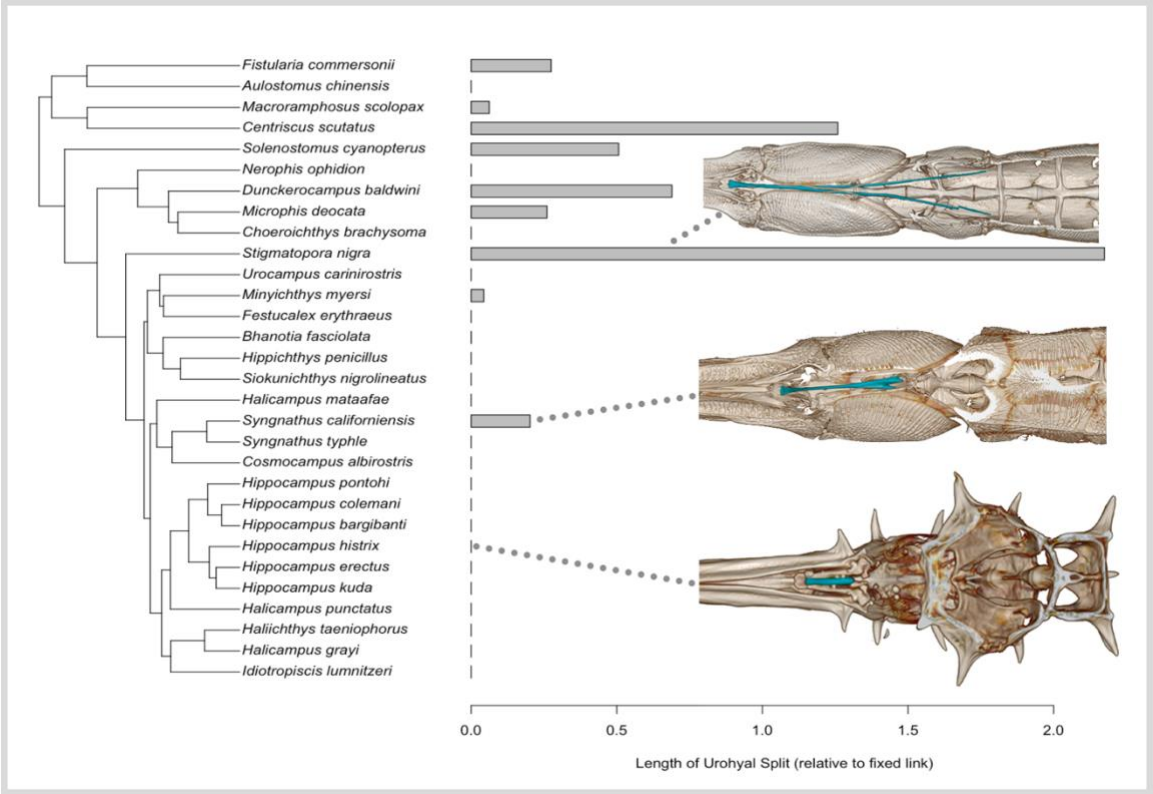

Figure 5. Length of the bifurcation of the urohyal bone compared across a phylogeny. The urohyal sometimes splits and becomes internal to the sternohyoideus and hypaxial muscles. In this form, it is evidently a heavy ossification of the sternohyoideus tendon. No seahorse possesses a split urohyal, but the trait appears more frequently in more basal groups. Urohyal split length has a significant phylogenetic signal.

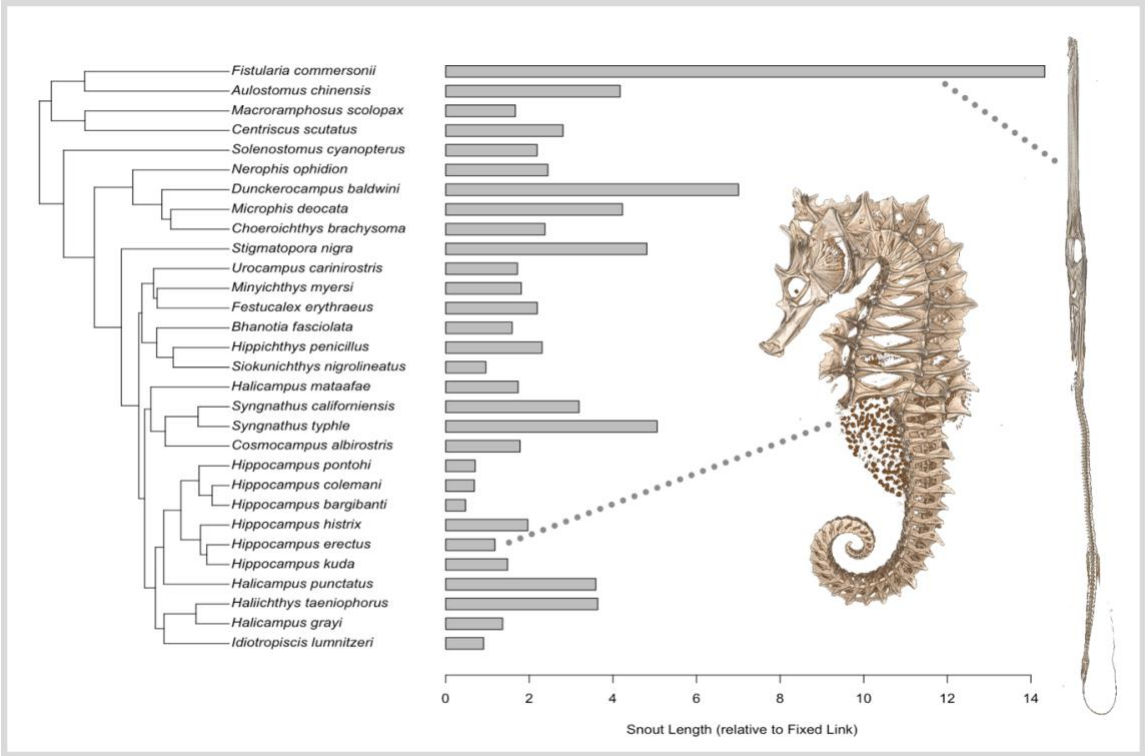

Figure 6. Phylogeny of species showing differences in snout length for different members of the Synagnthoidei suborder. Snout length is taken relative to pectoral girdle length to standardize for body size. *Fistularia comersonii* has a notably long snout and short pectoral girdle, resulting in a large corrected length. Pygmy seahorses have consistently shorter snouts than the main-group seahorses. Snout length has a significant phylogenetic signal across the suborder and family.

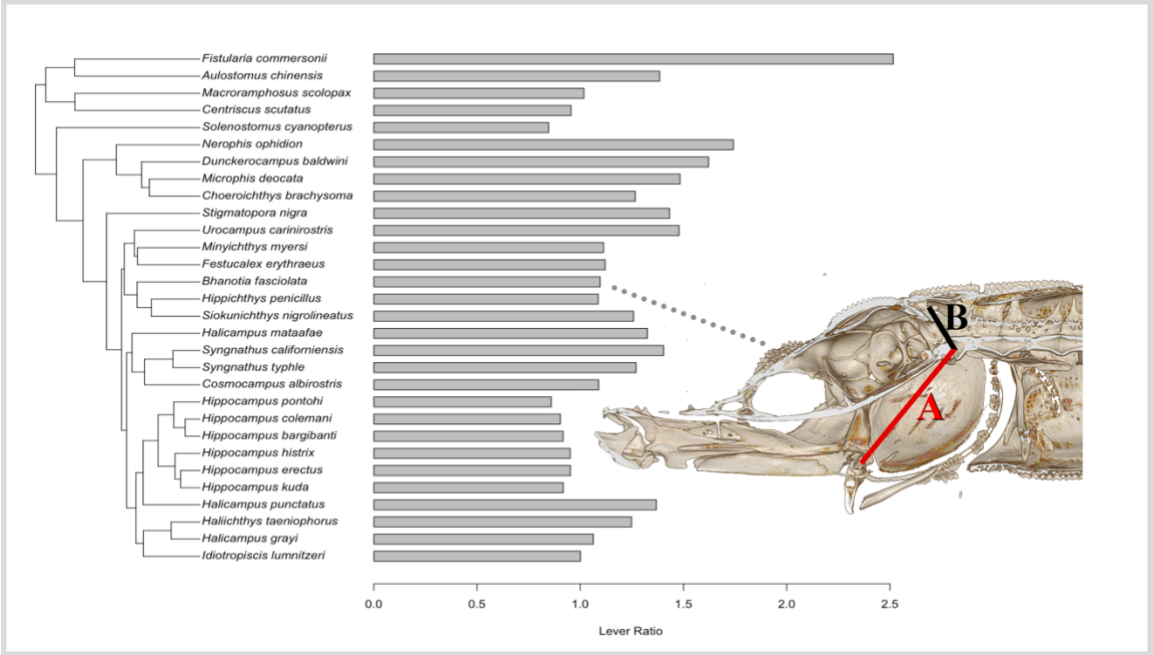

Figure 7. Lever ratio plotted across a phylogeny of Synagnthoidei. Lever ratio is the ratio of pectoral girdle length (A) divided by the distance from the fulcrum at the anterior protrusion of the first vertebrae to where the epaxial tendons connect to the supraoccipital (B). This ratio does not have a significant phylogenetic signal in this group, though variation is evident.

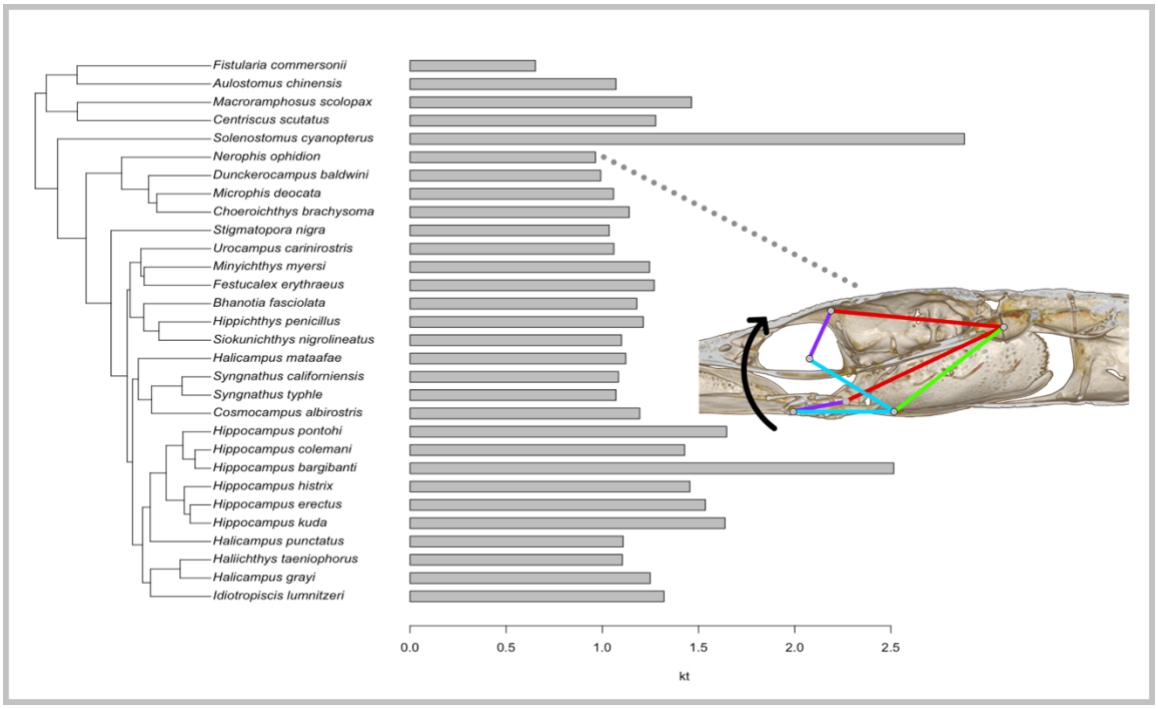

Figure 8. KT plotted across a phylogeny of Synathoidei. KT represents how much change in head angle elevation can be expected from a 4-bar linkage system, like the one used here to approximate a fish's feeding kinematics, for a given input angle. Here, the input angle was between the hyoid and urohyal, and increased by 50º. KT has a significant phylogenetic signal for all Synganthoidei, but a non-significant signal for Syngnathidae.

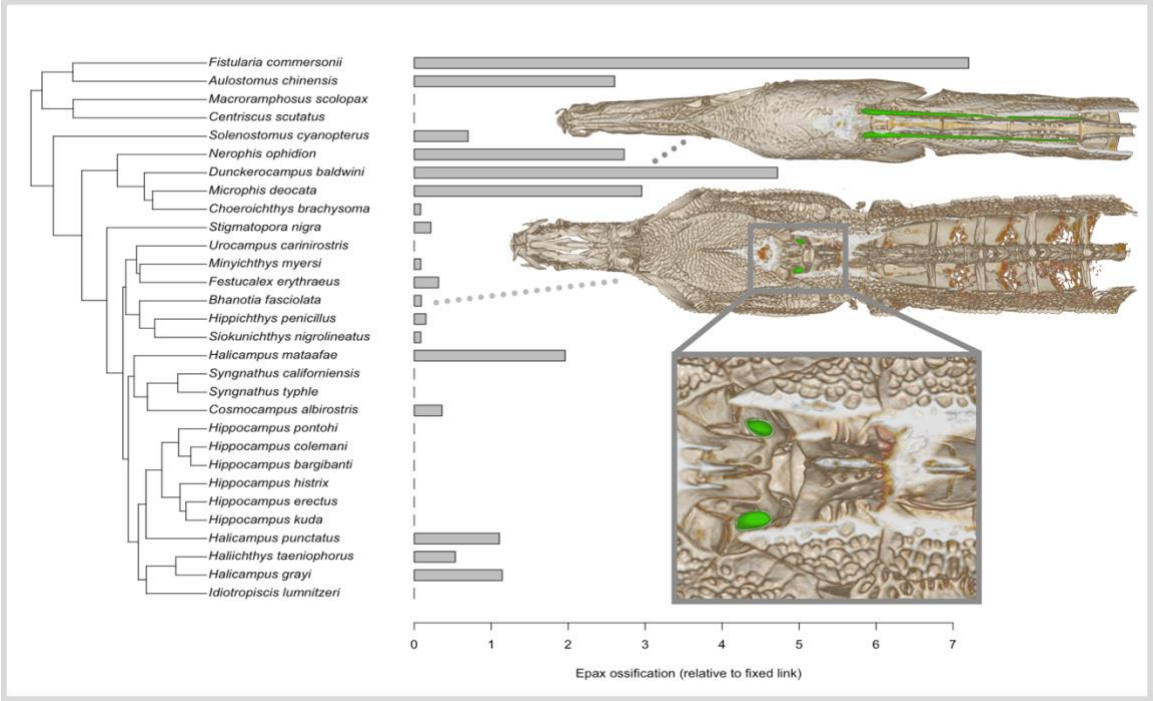

Figure 9. Epaxial ossification across a phylogeny of Syngnathoidei. Ossification of the epaxial tendons has a significant phylogenetic signal across the suborder and family. Additionally, ossification of the epaxial tendons may have repercussions on the ability of these fish to perform high-power feeding strikes. The elasticity of the epaxial tendons is critical to storing energy, which is then rapidly released in a feeding strike. Ossification of these tendons will reduce elasticity and may impact feeding capabilities.

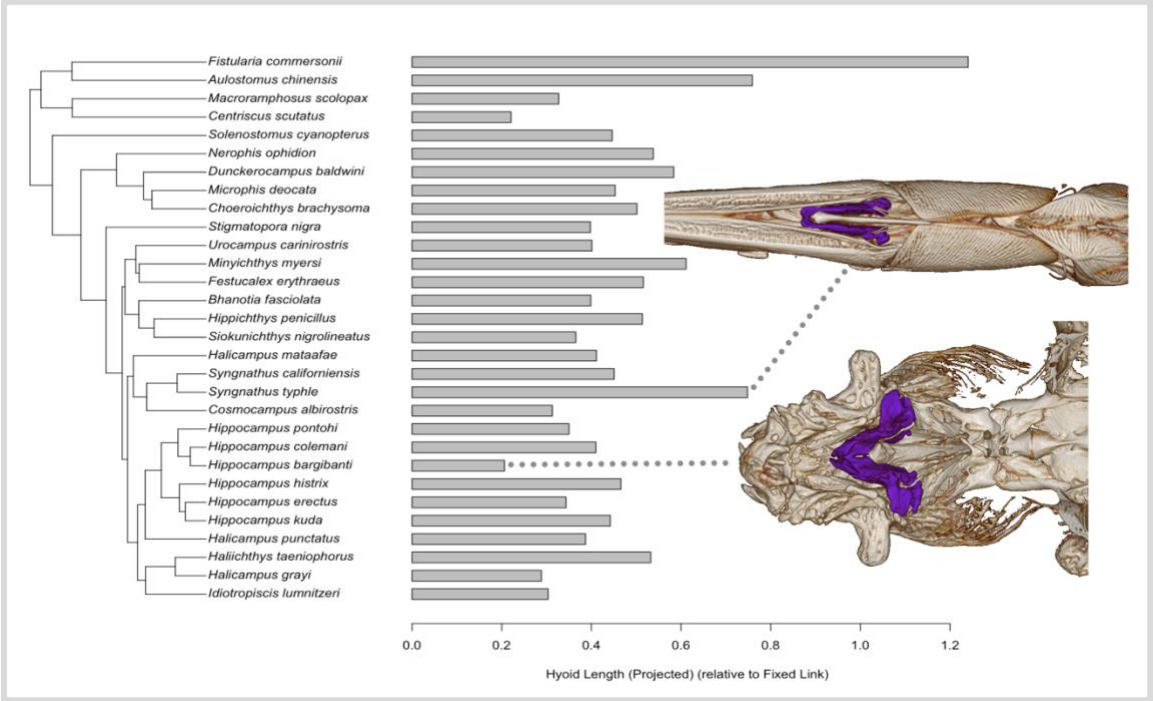

Figure 10. Length of the sagittally projected hyoid relative to the pectoral girdle over a phylogeny of Syngnathoidei. The length of the hyoid was measured by averaging the position of the joints between it and the hyomandibular and then computing the distance to the tip of the hyoid. *Hippocampus bargibanti* (pictured on the bottom) has a very short and wide hyoid as compared to many others from the suborder. The hyoid length has a significant phylogenetic signal across the suborder but not the family.

A PCA of all the functional lengths we measured that pertain to the suction feeding mechanism allows us to examine the major components of this system and view convergence or ancestral constraints on morphology. We connect all species on the PCA with a phylogeny to show their evolutionary relationships. PCA results on functional morphology, plotted as a phylomorphospace, show some clustering of related groups such as the Pygmy Seahorses and Main group Seahorses; however, some more distantly related species appear to converge on similar functional morphologies. The divergence of *Halicampus punctatus*, *Halicampus grayi*, *Haliichthys taeniophorus*, and *Idiotropiscis lumnitzeri* along with the genus *Hippocampus*, illustrates that a relatively rapid morphological divergence occurred in the evolutionary history of seahorses and their close relatives with regard to their suction-feeding related morphology.

Fistularia commersonii, *Aulostomus chinensis*, *Macroramphosus scolopax, Centriscus scutatus*, and *Solenostomus cyanopterus* represent an outgroup to the family Syngnathidae and are morphological outliers. PCAs are shown both with this group included and excluded in Figures 11-12, respectively.

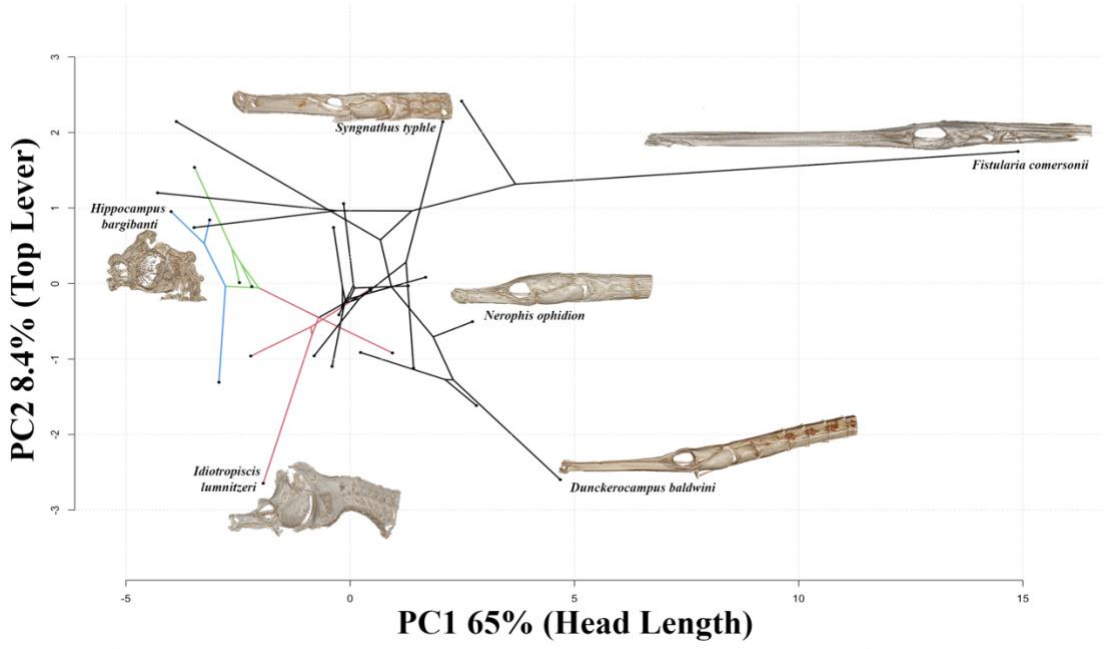

Figure 11. Phylomorphospace of functional traits across Syngnathoidei. Shown are dimensions 1 and 2 of a PCA on 21 functional lengths in 30 species across Syngnathoidei. PC1 primarily describes cranial and snout length, PC2 primarily describes the length of the 'Top Lever' or length from the anterior protrusion of the first vertebrae to the attachment of the epaxial tendons. The blue clade represents Pygmy seahorses, green the main group seahorses, and red includes genera *Idiotropiscus*, *Halicampus*, and *Haliichthys*. *Fistularia comersonii* represents an outgroup morphologically.

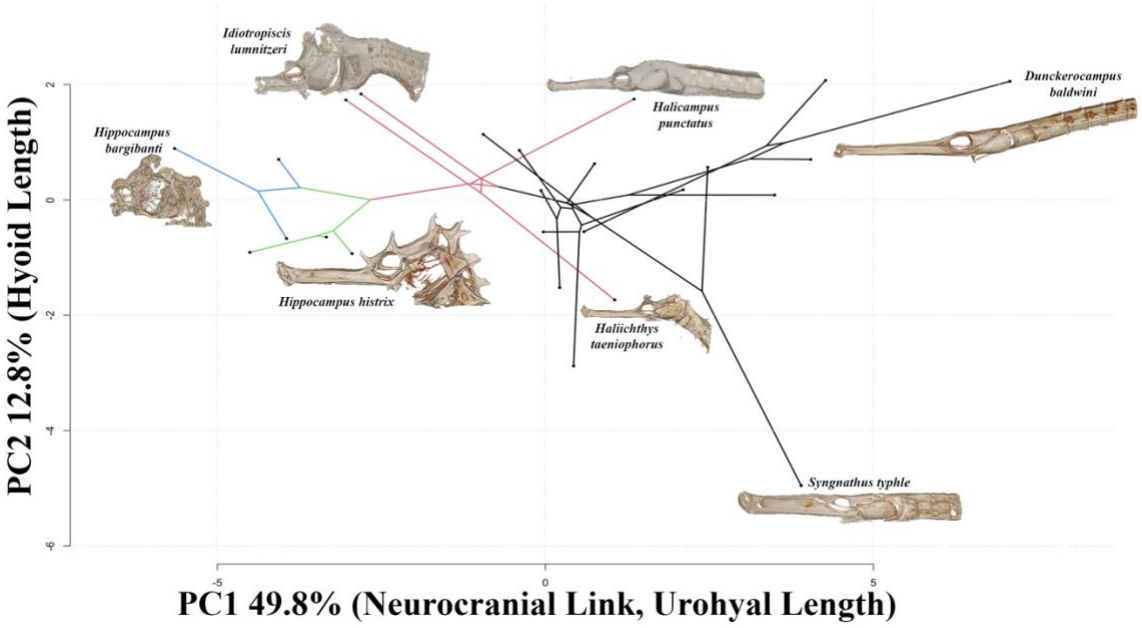

Figure 12. Phylomorphospace of the family Syngnathidae. Shown are dimensions 1 and 2 of a PCA on 21 functional lengths across 25 members of the Syngnathidae family. PC1 represents general cranial length, PC2 has major contributions from the hyoid Length, Mouth Height, and Top Lever, driven by the epaxials. As before, the blue clade represents Pygmy seahorses, green the main group seahorses, and red includes genera *Idiotropiscus*, *Halicampus*, and *Haliichthys*.

Urohyal length is functionally important in both the energy storage capacity and determining cranial movement in feeding strikes. It is therefore likely that the length of the urohyal has an influence on the system at large, which we test with an RDA. When urohyal length is taken as the sole explanatory variable for the remaining 20 functional lengths in an RDA using R package vegan (Oksanen et al., 2025), it explains 68.7% of variance in the other functional lengths. When the previously referenced outgroups are removed, this drops to 41.2% (Figure 13-14). We performed an ANOVA (R Core Team,

2025) on our RDA model, showing urohyal length as a significant predictor of other functional lengths with p=0.001.

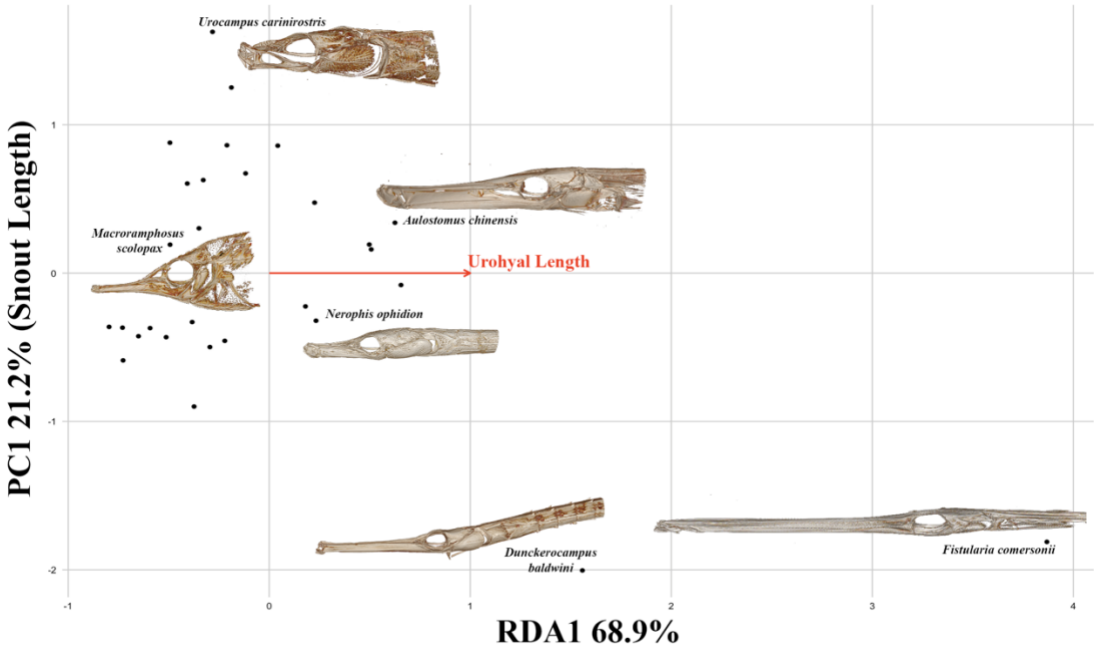

Figure 13. RDA with urohyal length as an explanatory variable of other functional lengths for our sample of the suborder Syngnathoidei. urohyal length alone can explain 68.9% of the variance in the other functional lengths. PC1 accounts for 21.2% of the variance and generally represents snout and head elongation.

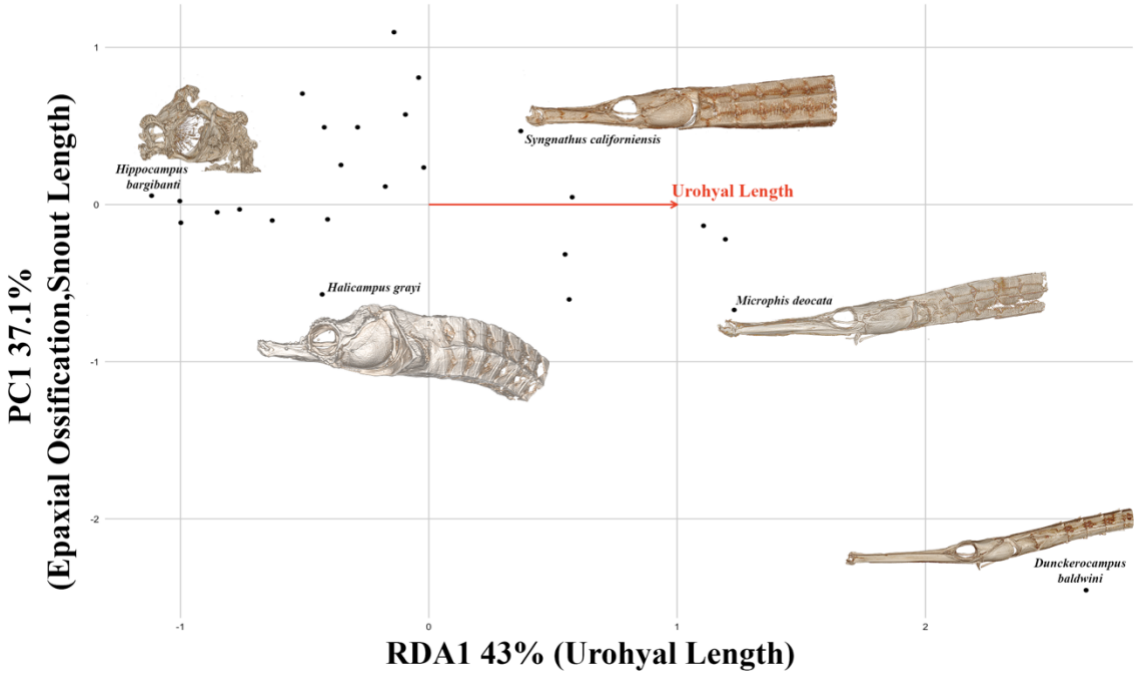

Figure 14. RDA with urohyal length as an explanatory variable of other functional lengths for our sample of the family Syngnathidae. urohyal length can explain 43% of the variance in the other functional lengths. PC1 accounts for 37.1% of the variance and generally represents snout and epaxial tendon ossification.

The 4 lengths defining the 4 bar linkage roughly approximate the linkage system central to pivot feeding in Syngnathids. As such, these lengths, which includes the urohyal length, should explain a large proportion of the variance in other functionally relevant morphological traits. All 4 bar linkage lengths together (urohyal length, pectoral girdle link, neurocranium-suspensorium link, hyoid length) explain 81.7% of the variance in the remaining 17 functional lengths: the variance explained by these four variables is 58.1% when non-Syngnathidae are removed. (Figure 14-16) An ANOVA (R Core Team, 2025) on these 4 lengths as predictors of the other functional lengths results in

significance values of $p=0.001$ for hyoid Length, $p < 0.01$ for the length of urohyal, $p < 0.05$ for the neurocranium-suspensoria link, and $p > 0.05$ ($p=0.294$) for the Pectoral Girdle, or 'Fixed' Link. For both urohyal and all four bars as explanatory variables, PC1 in the unconstrained analysis was composed primarily of Epaxial tendon ossification and Snout length.

We also performed an RDA using the Kinematic Transmission (KT) and Lever Ratio, defined as neurocranium-suspensoria linkage (the long lever arm) over the length from the anterior protrusion of the first vertebrae to the attachment of the epaxials (the short lever arm). These two variables explain 27.91% of the variance in the other functional lengths, excluding the 4-bar linkages, as these are used in calculating the explanatory variables. An ANOVA on these two variables as predictors of the other lengths yields $p<0.05$ for KT, and $p>0.05$ for the Lever ratio. Once species outside the family Syngnathidae are removed, KT and Lever ratio explain 37.98% of the variance in other lengths, with $p < 0.01$ for both KT and $p > 0.05$ for Lever Ratio under an ANOVA.

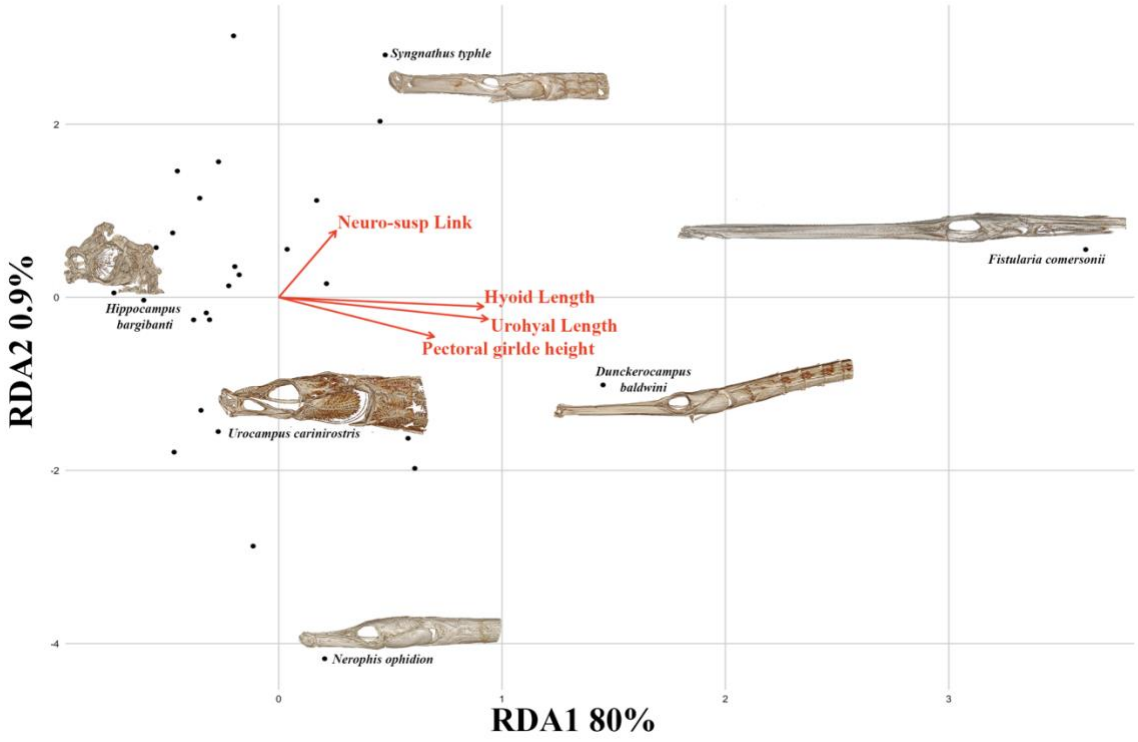

Figure 15. RDA with 4 bar linkage lengths as an explanatory variable of other functional lengths for our sample of the suborder Syngnathoidei. Altogether, the length of the hyoid, urohyal, pectoral girdle link, and neurocranium-suspensoria link can explain 81.7% of the variance in the remaining functional lengths.

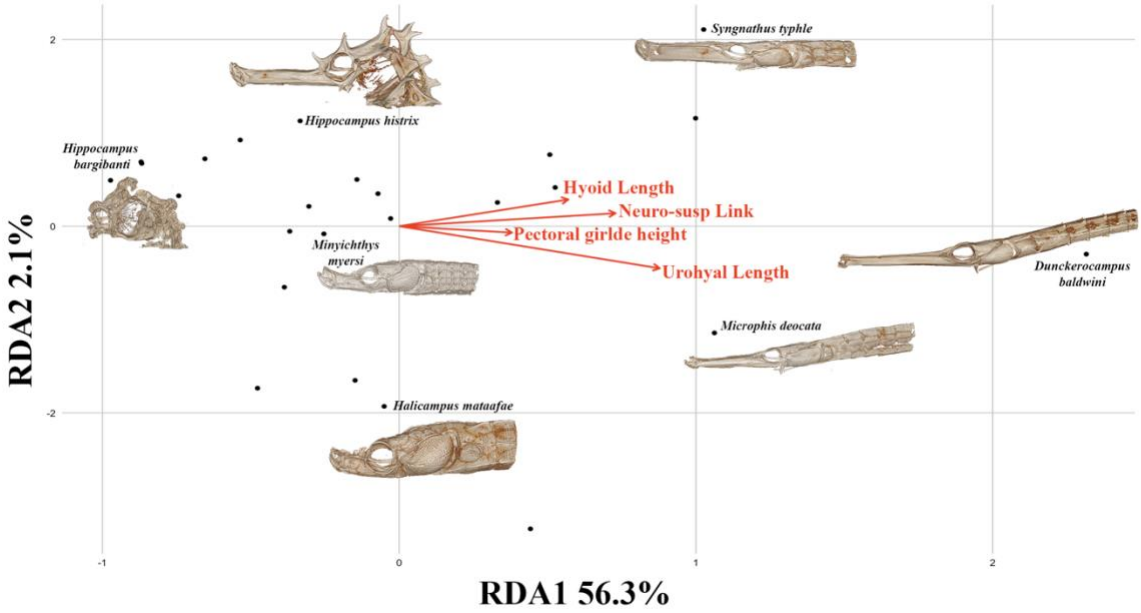

Figure 16. RDA with urohyal length as an explanatory variable of other functional lengths for our sample of the family Syngnathidae. Altogether, these 4 lengths can explain 59.9% of the variance in the remaining functional lengths.

Discussion

Syngnathoidei represent a diverse group of bony marine fish that inhabit a variety of habitats. They range from temperate to tropical waters and typically feed on small zooplankton, on whom their pivot-style suction feeding system is highly effective. Many are reef-associated and demersal (Whitehead 1986, Dawson 1985).

In this study, we have found a significant phylogenetic signal for a variety of functionally relevant lengths in the suborder Syngnathoidei. Of particular interest, urohyal length has a strong phylogenetic signal. Shortened urohyal length may act as an indicator of the presence of a larger sternohyoideus tendon, which can be used as a secondary source of elastic energy storage, supplementing the Epaxial tendons (Leysen

2011). The seahorses (*Hippocampus*) show a noticeably reduced urohyal when compared with pipefish (the remainder of the Syngnathidae family). However, notable exceptions arise in *Halicampus grayi* and *Idiotropiscis lumnitzeri*, which have relatively short urohyals. This group is closely related to *Hippocampus*; however, the direct sister to *Hippocampus* in our study sample, *Halicampus punctatus*, has a urohyal similar in length to that of typical pipefish, as does *Haliichthys taeniophorus*, another close relative. While urohyal length is relatively variable in the close relatives of *Hippocampus*, within the *Hippocampus* genus, the urohyal bone is consistently shorter than in pipefish. The sampled Pygmy Seahorses, *Hippocampus bargibanti*, *Hippocampus colemani*, and *Hippocampus pontohi*, show even shorter urohyals than the sampled main group seahorses (*Hippocampus kuda*, *Hippocampus histrix*, and *Hippocampus erectus*). *Hippocampus colemani* does not possess a urohyal bone. The length of the urohyal may be diagnostic of Pygmy Seahorses as compared to the main group Seahorses. The shape of urohyal in the Pygmies also represents a deviation from that of the non-pygmy *Hippocampus*, with Pygmies having more ball-shaped, or even flattened, disk-like urohyals, compared to the more familiar elongate shape in non-pygmy *Hippocampus*.

Epaxial ossification had a strong phylogenetic signal across our sample of Synganthiformes. No seahorses had epaxial ossification, and most pipefish had minimal ossification. A group of pipefish, including *Microphis deocata*, *Dunckerocampus baldwini*, and *Nerophis ophidion* have markedly long ossification of their epaxial tendons. *Aulostomus chinensis* and *Fistularia commersonii*, which represent the non-pipefish groups of Trumpetfish and Cornetfish, also have long ossification of their epaxials. The epaxial tendons are used in elastic energy storage in Syngnathidae, (Divi et

al., 2020; Longo et al., 2019; Longo et al., 2018; Van Wassenbergh et al. 2013; Van Wassenbergh et al., 2008), and so a large ossification of this tendon indicates a possible loss or reduction in the ability of these fish to use elastic energy storage to power feeding strikes. Further inquiry into the lifestyles of these fish is needed to determine the consequences of this difference.

We found a significant phylogenetic signal for KT only for the suborder as a whole. The KT can be interpreted as the gearing of the cranial system, with a lower KT value indicating more output angle for the same input. This results in more rapid strikes, at the cost of needing additional power (Muller et al., 1987). With the cranial system modeled as a 4-bar linkage, seahorses can be seen to have higher KT values than pipefish, which is consistent with their high-powered, fast-feeding strikes (Avidan et al., 2023; Roos et al., 2009).

In both PCAs of both Syngnathidae and Syngnathoidei, we can observe high degrees of non-phylogenetically based clustering, as we see non-closely related species are often closer in morphospace than closer relatives. This may indicate convergence based on ecology (Stayton, 2015) rather than functional traits being primarily determined by ancestry.

Urohyal length alone accounts for 68.9% of the variance in other functional lengths in members of Syngnathoidie and 43% in Syngnathidae. This relatively large variance explained by this one length implies a high degree of importance in its involvement with the functional system of suction feeding. The differences between pipefish and seahorse feeding strike mechanisms are amplified by this finding. Large differences in urohyal length are evident between the groups, and changes in this length

can account for changes in other functional traits. In this way, the urohyal is placed as a centrally important part of determining the entire suction feeding system in Syngnathoidei. We note that relative urohyal length may vary to some extent within a single species, as the urohyal represents an ossification often internal to the sternohyoideus tendon.

To expand further on the importance of the four-bar approximation for a suction feeding model, when all four are used as explanatory variables of the remaining lengths in our RDA, these 4 lengths can together explain 81.7% in Syngnathoidei and 59.9% in Syngnathidae of the variance in the other measurements. This validates the role of the four-bar linkage system, or at least its constituent parts, as central to the entire functional system. Snout length and Epaxial ossification are the major contributors to the first unconstrained axis in both the urohyal and 4-bar RDAs. This means that both the urohyal length and the 4 bar lengths in general have a large correlation with other functional features. Syngnathids encounter significant hydrodynamical challenges when rapidly elevating their heads in a feeding strike (Van Wassenbergh et al., 2008). Epaxial ossification, which may constrain elastic energy storage in the epaxial tendons (O'Brien et al. 2012, Van Wassenbergh et al., 2008) is likely to interplay with traits immediately involved in power storage, amplification, and performing feeding strikes. This, too, is evidenced by the large contribution to PC1 of both RDAs.

The feeding mechanics of seahorses, pipefish, and other members of the suborder Syngnathoidei are highly complex dynamic systems that, despite extensive study, are still not fully understood. A high degree of complexity, many moving parts, and the suspension of the entire system in a fluid make many avenues of study exceedingly

difficult. However, the application of comparative methods in the light of the well-resolved taxonomy allows a different perspective to be taken than a purely mechanical one. In comparing different groups within Synathoidei, all sharing commonalities regarding morphology and mechanics, differences become more evident. Variations in traits between different groups, such as pipefish and seahorses, can shed light not only on taxonomically diagnostic form, but on the evolution of function. Future inquiries into the consequences of epaxial tendon ossification on energy storage, as well as the continuation of studies on the role of the sternohyoideus tendon and urohyal in storing elastic energy in seahorses, are necessary to better understand the dynamics of pivot feeding in the group, as well as understanding how different regimes of this feeding stratagem evolved within the family, suborder, and order.

Appendix Table 1a. CT scan metadata for specimens. Some entries are unknown or not applicable and left blank. The scanning facility, specimen code, resolution, and CT scanner model are listed.

Species	Scanned by	Specimen	Resolution (um)	Device
Hippocampus kuda	Karel F Liem Bioimaging Facility	CAS 20004	20	Bruker SkyScan 1273
Urocampus carinirostris	Karel F Liem Bioimaging Facility	CAS 241506	6.7	Bruker SkyScan 1273
Cosmocampus albirostris	Florida Museum of Natural History, University of Florida	UF:Fish:233194	20	General Electric phoenix v|tome|x m 240
Hippichthys penicillus	Karel F Liem Bioimaging Facility	SAIAB 75221	16	Bruker SkyScan1273
Halicampus punctatus	Karel F Liem Bioimaging Facility	FMNH 120903	24.1	Bruker SkyScan1273
Idiotropiscis lumnitzeri	Karel F Liem Bioimaging Facility	AM	8.1	Bruker SkyScan1273
Minyichthys myersi	Karel F Liem Bioimaging Facility	AM 21918	4	Bruker SkyScan1273
Nerophis ophidion	UF Nanoscale Research Facility	YPM:VZ:YPM ICH 003569	27.6	General Electric phoenix v|tome|x m 240
Macroramphosus scolopax	UF Nanoscale Research Facility	UF:Fish:177459	32	General Electric phoenix v|tome|x m 240
Bhanotia fasciolata	UF Nanoscale Research Facility	UF:Fish:23759	7.2	General Electric phoenix v|tome|x m 240
Stigmatopora nigra	Karel F Liem Bioimaging Facility	NZ AKL	6	Bruker SkyScan 1273
Hippocampus bargibanti	Karel F Liem Bioimaging Facility		6.7	Bruker SkyScan 1273
Hippocampus histrix	Karel F Liem Bioimaging Facility	ANSP 193114	37	Bruker SkyScan 1273
Siokunichthys nigrolineatus	Karel F Liem Bioimaging Facility	CAS Philippines2011	11	Bruker SkyScan 1273
Syngnathus californiensis	Karel F Liem Bioimaging Facility		6	Bruker SkyScan 1273
Hippocampus pontohi	Karel F Liem Bioimaging Facility		8.8	Bruker SkyScan 1273
Festucalex erythraeus	Karel F Liem Bioimaging Facility	UMMZ	6	Bruker SkyScan 1273
Halicampus grayi	Karel F Liem Bioimaging Facility	LSU 14096.7	25	Bruker SkyScan 1273
Hippocampus colemani	Karel F Liem Bioimaging Facility		12.7	Bruker SkyScan 1273
Hippocampus minotaur	Karel F Liem Bioimaging Facility	CAS	7.1	Bruker SkyScan 1273
Microphis deocata	Karel F Liem Bioimaging Facility	UMMZ 208669	15.5	Bruker SkyScan 1273
Hippocampus erectus	Karel F Liem Bioimaging Facility		71.1	Bruker SkyScan 1273
Dunckerocampus baldwini	Karel F Liem Bioimaging Facility	CAS 13424	10	Bruker SkyScan 1273
Campichthys galei	Karel F Liem Bioimaging Facility	USNM 216313	4.5	Bruker SkyScan 1273
Centriscus scutatus	UF Nanoscale Research Facility	SIO:Marine Vertebrates:70-274	17	General Electric phoenix v|tome|x m 240
Solenostomus cyanopterus	Karel F Liem Bioimaging Facility	SAIAB 14841	9	Bruker SkyScan 1273
Haliichthys taeniophorus	Karel F Liem Bioimaging Facility	SIO 25-44	23	Bruker SkyScan 1273
Aulostomus chinensis	Karel F Liem Bioimaging Facility	UW 27054	12	Bruker SkyScan 1273
Syngnathus typhle	Karel F Liem Bioimaging Facility	UW 8205	20	Bruker SkyScan 1273
Fistularia commersonii	Karel F Liem Bioimaging Facility	UW 8495	20	Bruker SkyScan 1273
Choeroichthys brachysoma	Karel F Liem Bioimaging Facility	UW SLU900	4.3	Bruker SkyScan 1273

Halicampus mataafae	Karel F Liem Bioimaging Facility	UW 22675	8.5	Bruker SkyScan 1273

Appendix Table 1b. Continuation of Table 1a, voltage, current, exposure time, step size, filter, and citation when applicable are listed.

Species	Voltage (kV)	Current (uA)	Exposure time (ms)	Step	Filter	Citation
Hippocampus kuda	50	200	103	0.63217 deg, Continuous	No Filter	
Urocampus carinirostris	65	123	1100	0.3	1mm Al	
Cosmocampus albirostris	70	200	200			University of Florida provided access to these data provided access to these data , the collection of which was funded by oVert TCN. The files were downloaded from www.MorphoSource.org, Duke University.; Blackburn, D.C., et al. 2024. Increasing the impact of vertebrate scientific collections through 3D-imaging: the openVertebrate (oVert) Thematic Collections Network. BioScience 74: 169–186. https://doi.org/10.1093/biosci/biad120
Hippichthys penicillus	50	200	157	0.31783 deg, Continuous	No Filter	
Halicampus punctatus	65	123	1300	0.3 deg	1mm Al	
Idiotropiscis lumnitzeri	65	123	1170	0.3 deg	1mm Al	
Minyichthys myersi	65	100	189	0.2 deg	No Filter	
Nerophis ophidion	60	200	200			Yale University provided access to these data , the collection of which was funded by oVert TCN; NSF DBI-1701714; NSF DBI-1701769.. The files were downloaded from www.MorphoSource.org, Duke University.; Blackburn, D.C., et al. 2024. Increasing the impact of vertebrate scientific collections through 3D-imaging: the openVertebrate (oVert) Thematic Collections Network. BioScience 74: 169–186. https://doi.org/10.1093/biosci/biad120
Macroramphosus scolopax	70	200	200			University of Florida provided access to these data provided access to these data , the collection of which was funded by oVert TCN. The files were downloaded from www.MorphoSource.org, Duke University.; Blackburn, D.C., et al. 2024. Increasing the impact of vertebrate scientific collections through 3D-imaging: the openVertebrate (oVert) Thematic Collections Network. BioScience 74: 169–186. https://doi.org/10.1093/biosci/biad120
Bhanotia fasciolata	80	200	250			Blackburn, D.C., et al. 2024. Increasing the impact of vertebrate scientific collections through 3D-imaging: the openVertebrate (oVert) Thematic Collections Network. BioScience 74: 169–186. https://doi.org/10.1093/biosci/biad120
Stigmatopora nigra	65	100	283	0.2 deg	0.5mm Al	
Hippocampus bargibanti	65	123				
Hippocampus histrix	80	200	57	0.25 deg	0.5mm Al	
Siokunichthys nigrolineatus	130	70	110	0.28275 deg, Continuous	0.5mm Al	
Syngnathus californiensis	65	100	283	0.2 deg	0.5mm Al	
Hippocampus pontohi						
Festucalex erythraeus	65	100	283	0.77991 deg, Continuous	0.5mm Al	
Halicampus grayi						
Hippocampus colemani						
Hippocampus minotaur						

Microphis deocata	90	166	108	0.27064 deg, Continuous	1mm Al	
Hippocampus erectus						
Dunckerocampus baldwini	50	200	103	0.63368 deg, Continuous	No Filter	
Campichthys galei	65	165	283	0.2 deg	0.5mm Al	
Centriscus scutatus	80	200	200			
Solenostomus cyanopterus	65	100	283	0.15 deg	0.5mm Al	
Haliichthys taeniophorus	65	100	283	0.2 deg	0.5mm Al	
Aulostomus chinensis	65	100	283	0.2 deg	0.5mm Al	
Syngnathus typhle	65	100	283	0.2 deg	0.5mm Al	
Fistularia commersonii	65	100	283	0.2 deg	0.5mm Al	
Choeroichthys brachysoma	65	100	283	0.2 deg	0.5mm Al	
Halicampus mataafae	65	100	283	0.2 deg	0.5mm Al	

Appendix Table 2a. Functional lengths (mm) relating to feeding mechanics measured across members of Syngnathoidei.

	Mouth Width	Mouth Height	Snout Length	hyoid Side	hyoid Width	urohyal Length	Spring +urohyal	Body Height	Neurcranium Link, nonsuspensora	suspensoria height	Top Lever	Epax ossification	Dentary Length
Hippocampus kuda	2.953	5.763	19.365	6.114	4.194	2.588	9.688	13.091	5.545	7.358	4.482	0.000	4.173
Urocampus carinirostris	0.462	0.988	2.242	0.579	0.461	1.475	2.235	1.305	1.312	0.866	0.551	0.000	0.831
Cosmocampus albirostris	1.423	1.821	7.342	1.741	2.146	2.538	3.464	4.120	2.966	2.058	1.339	1.492	1.589
Hippichthys penicillus	1.009	2.213	8.615	2.086	1.420	3.422	4.877	3.735	2.760	1.719	1.394	0.565	2.180
Halicampus punctatus	0.985	1.817	12.013	1.433	1.293	3.675	4.326	3.343	2.694	2.200	1.517	3.695	1.628
Idiotropiscis lumnitzeri	0.733	1.273	2.625	1.101	1.170	0.309	1.188	2.888	1.518	1.537	1.602	0.000	0.931
Minyichthys myersi	0.140	0.385	0.966	0.341	0.214	0.389	0.676	0.534	0.423	0.277	0.163	0.046	0.385

Nerophis ophidion	0.826	1.238	4.907	1.188	0.954	1.598	3.329	2.006	2.345	1.418	0.808	5.474	1.258
Macroramphosus scolopax	1.926	2.979	25.994	5.300	3.087	7.641	9.435	15.577	4.961	11.776	4.478	0.000	3.418
Bhanotia fasciolata	0.768	1.025	3.351	0.981	1.117	1.429	2.033	2.107	1.526	1.167	0.858	0.193	0.940
Stigmatopora nigra	0.261	0.417	3.425	0.314	0.312	0.785	1.377	0.712	0.768	0.351	0.222	0.154	0.525
Hippocampus bargibanti	0.618	1.126	1.567	0.837	0.890	0.173	0.777	3.291	1.603	2.264	0.609	0.000	0.713
Hippocampus histrix	1.268	3.574	15.137	3.726	2.009	2.491	6.915	7.708	3.317	4.329	2.792	0.000	2.406
Siokunichthys nigrolineatus	0.942	1.021	1.723	0.771	0.815	1.239	2.702	1.792	1.640	0.935	0.425	0.154	0.850
Syngnathus californiensis	1.050	2.004	10.193	1.624	1.619	3.375	5.104	3.194	3.365	1.604	1.523	0.000	1.817
Hippocampus pontohi	0.596	0.844	1.338	0.727	0.616	0.175	0.405	1.892	0.822	0.897	0.779	0.000	0.539
Festucalex erythraeus	0.678	1.416	5.663	1.475	1.235	1.577	2.709	2.585	1.916	1.334	0.987	0.817	1.349
Halicampus grayi	1.267	1.710	7.864	1.990	2.033	0.771	4.846	5.771	3.723	2.858	2.101	6.602	1.586
Hippocampus colemani	0.724	0.778	1.300	0.901	0.881	0.000	0.204	1.894	0.996	0.811	0.308	0.000	0.582
Hippocampus minotaur	0.764	1.296	2.437	1.060	1.003	0.274	1.337	3.879	1.683	1.938	1.691	0.000	1.036
Microphis deocata	1.305	1.768	12.495	1.453	1.658	3.629	4.352	2.955	3.373	1.669	1.508	8.731	1.913
Hippocampus erectus	2.053	4.125	12.444	4.075	3.526	1.812	6.737	10.548	4.934	5.666	1.470	0.000	3.096
Dunckerocampus baldwini	1.124	1.437	17.358	1.670	1.760	2.793	4.173	2.478	3.155	1.299	1.464	11.696	1.300
Campichthys galei	3.590	6.410	16.458	5.071	4.219	5.487	9.145	10.608	8.279	5.112	3.691	2.255	4.983
Centriscus scutatus	1.387	1.630	33.568	2.839	1.978	5.012	8.396	11.958	4.675	7.149	2.283	0.000	0.973
Solenostomus cyanopterus	1.054	4.930	22.509	4.621	1.332	3.949	3.955	10.291	4.708	4.545	1.700	7.203	5.228
Haliichthys taeniophorus	1.126	3.841	23.960	3.761	2.519	4.835	10.478	6.588	5.623	3.354	2.155	3.528	3.072
Aulostomus chinensis	1.060	8.535	34.355	6.549	2.267	11.095	15.083	8.229	6.435	5.332	2.861	21.425	10.611

Syngnathus typhle	1.222	4.729	24.619	3.809	2.081	5.241	9.232	4.866	4.032	2.751	1.522	0.000	5.121
Fistularia commersonii	3.098	5.223	58.611	5.627	5.198	11.551	13.422	4.090	7.283	3.606	2.087	29.458	9.473
Choeroichthys brachysoma	0.353	0.893	4.497	1.005	0.597	2.055	2.578	1.892	1.523	1.062	0.873	0.158	1.004
Halicampus mataafae	0.736	1.405	4.170	1.111	0.912	2.358	2.741	2.403	2.307	1.595	0.814	4.715	1.169

Appendix Table 2b.

	Pectoral Girdle Width	Neuro-Susp Link	urohyal Split Length	Projected hyoid Length	Neurocranial susp link projected	Fixed Link Projected	Pect Girdle - hyoid Mid Joint	Lever projected
Hippocampus kuda	6.478	12.057	0.000	5.787	12.012	12.889	4.063	3.895
Urocampus carinirostris	0.819	1.946	0.000	0.524	1.930	1.303	1.717	0.479
Cosmocampus albirostris	3.200	4.543	0.000	1.290	4.487	3.992	2.856	1.214
Hippichthys penicillus	2.109	4.115	0.000	1.919	4.060	3.631	2.961	1.283
Halicampus punctatus	2.953	4.528	0.000	1.294	4.573	3.327	3.050	1.478
Idiotropiscis lumnitzeri	1.331	2.892	0.000	0.876	2.890	2.851	1.374	1.572
Minyichthys myersi	0.286	0.602	0.023	0.327	0.595	0.525	0.363	0.145
Nerophis ophidion	0.984	3.480	0.000	1.080	3.495	1.946	2.251	0.799
Macroramphosus scolopax	2.847	15.950	0.972	5.098	15.850	15.495	4.503	4.420
Bhanotia fasciolata	1.298	2.315	0.001	0.840	2.310	2.071	1.813	0.816
Stigmatopora nigra	0.430	1.020	1.548	0.283	1.019	0.695	1.095	0.231
Hippocampus bargibanti	1.754	3.165	0.000	0.679	3.018	3.270	0.295	0.580
Hippocampus histrix	3.813	7.352	0.001	3.591	7.334	7.598	3.411	2.616
Siokunichthys nigrolineatus	0.942	2.285	0.000	0.655	2.255	1.789	2.060	0.348

Syngnathus californiensis	2.238	4.507	0.647	1.440	4.483	3.168	3.669	1.387
Hippocampus pontohi	0.884	1.629	0.000	0.662	1.626	1.875	0.621	0.762
Festucalex erythraeus	1.959	2.880	0.000	1.333	2.897	2.533	1.376	0.905
Halicampus grayi	3.675	6.169	0.000	1.665	6.136	5.745	3.204	2.000
Hippocampus colemani	0.910	1.702	0.000	0.777	1.711	1.875	0.939	0.285
Hippocampus minotaur	1.085	3.358	0.000	0.917	3.370	3.841	0.632	1.587
Microphis deocata	2.226	4.400	0.769	1.338	4.383	2.898	3.738	1.322
Hippocampus erectus	4.805	10.040	0.000	3.623	10.045	10.449	3.309	1.394
Dunckerocampus baldwini	1.356	4.058	1.709	1.447	4.018	2.364	4.003	1.284
Campichthys galei	6.632	11.408	0.000	4.567	11.411	10.420	4.635	3.412
Centriscus scutatus	1.992	11.406	15.053	2.642	11.424	11.981	5.917	2.309
Solenostomus cyanopterus	1.842	8.810	5.213	4.595	8.712	10.242	1.548	1.604
Haliichthys taeniophorus	3.727	7.849	0.000	3.507	8.224	6.288	7.147	1.945
Aulostomus chinensis	4.562	10.943	0.000	6.245	11.394	8.183	8.868	3.009
Syngnathus typhle	2.867	6.225	0.000	3.641	6.180	4.773	5.846	1.256
Fistularia commersonii	5.326	10.474	1.125	5.073	10.291	3.952	8.520	2.135
Choeroichthys brachysoma	0.991	2.454	0.000	0.949	2.396	1.845	1.632	0.805
Halicampus mataafae	1.454	3.179	0.000	0.988	3.184	2.351	1.755	0.810

Acknowledgements

We would like to thank the Karel F Liem Bioimaging Center at the University of Washington, Friday Harbor Laboratories, for allowing us to use their CT scanner to facilitate this research. We would also like to thank Dr. Adam Summers and everyone in Lab 8 at Friday Harbor for their support, as well as the entire Friday Harbor Laboratories community for their dedication to providing an incredible research facility in an incredible location.

This research was supported by NSF Grant DBI-2149705

References

3D slicer image computing platform. (n.d.). Retrieved July 25, 2025, from https://www.slicer.org/

Avidan, C., Day, S. W., & Holzman, R. (2023). A power amplification dyad in seahorses. *Proceedings of the Royal Society*.

Camp, A. L., Roberts, T. J., & Brainerd, E. L. (2015). Swimming muscles power suction feeding in largemouth bass. *Proceedings of the National Academy of Sciences*, *112*(28), 8690–8695.

Camp, A. L., Roberts, T. J., & Brainerd, E. L. (2018). Bluegill sunfish use high power outputs from axial muscles to generate powerful suction-feeding strikes. *Journal of Experimental Biology*, *221*(11), jeb178160.

Carroll, A. M., & Wainwright, P. C. (2006). Muscle function and power output during suction feeding in largemouth bass, Micropterus salmoides. *Comparative Biochemistry and Physiology. Part A, Molecular & Integrative Physiology*, *143*(3), 389–399. https://doi.org/10.1016/j.cbpa.2005.12.022

Carroll, A. M., Wainwright, P. C., Huskey, S. H., Collar, D. C., & Turingan, R. G. (2004). Morphology predicts suction feeding performance in centrarchid fishes. *Journal of Experimental Biology*, *207*(22), 3873–3881. https://doi.org/10.1242/jeb.01227

Dawson, C. E. (Charles E.). (1985). *Indo-Pacific pipefishes: (Red Sea to the Americas)*. Ocean Springs, Miss., U.S.A. : Gulf Coast Research Laboratory.

Day, S. W., Higham, T. E., Cheer, A. Y., & Wainwright, P. C. (2005). Spatial and temporal patterns of water flow generated by suction-feeding bluegill sunfish

Lepomis macrochirus resolved by Particle Image Velocimetry. *Journal of Experimental Biology*, *208*(14), 2661–2671. https://doi.org/10.1242/jeb.01708

Divi, S., Ma, X., Ilton, M., St. Pierre, R., Eslami, B., Patek, S., & Bergbreiter, S. (2020). Latch-based control of energy output in spring actuated systems. *Journal of the Royal Society Interface*, *17*(168), 20200070.

Fedorov, A., Beichel, R., Kalpathy-Cramer, J., Finet, J., Fillion-Robin, J.-C., Pujol, S., Bauer, C., Jennings, D., Fennessy, F., Sonka, M., Buatti, J., Aylward, S., Miller, J. V., Pieper, S., & Kikinis, R. (2012). 3D Slicer as an image computing platform for the Quantitative Imaging Network. *Magnetic Resonance Imaging*, *30*(9), 1323–1341. https://doi.org/10.1016/j.mri.2012.05.001

Lê, S., Josse, J., & Husson, F. (2008). FactoMineR: A Package for Multivariate Analysis. *Journal of Statistical Software*, *25*(1), 1–18. https://doi.org/10.18637/jss.v025.i01

Leysen, H., J Christiaens, & KEGEL, B. (2011). Musculoskeletal structure of the feeding system and implications of snout elongation in Hippocampus reidi and Dunckerocampus dactyliophorus. *J. Fish Biol*, *78*, 1799–1823.

Longo, S., Cox, S., Azizi, E., Ilton, M., Olberding, J., St Pierre, R., & Patek, S. (2019). Beyond power amplification: Latch-mediated spring actuation is an emerging framework for the study of diverse elastic systems. *Journal of Experimental Biology*, *222*(15), jeb197889.

Longo, S. J., Goodearly, T., & Wainwright, P. C. (2018). Extremely fast feeding strikes are powered by elastic recoil in a seahorse relative, the snipefish, Macroramphosus scolopax. *Proceedings of the Royal Society B: Biological Sciences*, *285*(1882), 20181078.

Muller, M. (1987). Optimization principles applied to the mechanism of neurocranium levation and mouth bottom depression in bony fishes (Halecostomi). *Journal of Theoretical Biology*, *126*(3), 343–368. https://doi.org/10.1016/S0022-5193(87)80241-2

Muller, M., Osse, J. W. M., & Verhagen, J. H. G. (1982). A quantitative hydrodynamical model of suction feeding in fish. *Journal of Theoretical Biology*, *95*(1), 49–79. https://doi.org/10.1016/0022-5193(82)90287-9

O'Brien, E. J. O., Frank, C. B., Shrive, N. G., Hallgrímsson, B., & Hart, D. A. (2012). Heterotopic mineralization (ossification or calcification) in tendinopathy or following surgical tendon trauma. *International Journal of Experimental Pathology*, *93*(5), 319–331. https://doi.org/10.1111/j.1365-2613.2012.00829.x

Oksanen, J., Simpson, G. L., Blanchet, F. G., Kindt, R., Legendre, P., Minchin, P. R., O'Hara, R. B., Solymos, P., Stevens, M. H. H., Szoecs, E., Wagner, H., Barbour, M., Bedward, M., Bolker, B., Borcard, D., Borman, T., Carvalho, G., Chirico, M., Caceres, M. D., … Weedon, J. (2025). *vegan: Community Ecology Package*. https://doi.org/10.32614/CRAN.package.vegan

Olsson, K. H., Gurka, R., & Holzman, R. (2022). Trophic guilds of suction-feeding fishes are distinguished by their characteristic hydrodynamics of swimming and feeding. *Proceedings of the Royal Society B: Biological Sciences*, *289*(1966), 20211968. https://doi.org/10.1098/rspb.2021.1968

R Core Team. (2025). *R: A Language and Environment for Statistical Computing*. R Foundation for Statistical Computing. https://www.R-project.org/

Revell, L. J. (2024). phytools 2.0: An updated R ecosystem for phylogenetic comparative methods (and other things). *PeerJ*, *12*, e16505. https://doi.org/10.7717/peerj.16505

Rolfe, S., Pieper, S., Porto, A., Diamond, K., Winchester, J., Shan, S., Kirveslahti, H., Boyer, D., Summers, A., & Maga, A. M. (2021). SlicerMorph: An open and extensible platform to retrieve, visualize and analyse 3D morphology. *Methods in Ecology and Evolution*, *12*(10), 1816–1825. https://doi.org/10.1111/2041-210X.13669

Roos, G., Leysen, H., Van Wassenbergh, S., Herrel, A., Jacobs, P., Dierick, M., Aerts, P., & Adriaens, D. (2009). Linking Morphology and Motion: A Test of a Four-Bar Mechanism in Seahorses. *Physiological and Biochemical Zoology*, *82*(1), 7–19. https://doi.org/10.1086/589838

Roos, G., Van Wassenbergh, S., Herrel, A., & Aerts, P. (2009). Kinematics of suction feeding in the seahorse Hippocampus reidi. *Journal of Experimental Biology*, *212*(21), 3490–3498. https://doi.org/10.1242/jeb.033050

Short, G. A., & Trnski, T. (2021). A New Genus and Species of Pygmy Pipehorse from Taitokerau Northland, Aotearoa New Zealand, with a Redescription of Acentronura Kaup, 1853 and Idiotropiscis Whitley, 1947 (Teleostei, Syngnathidae). *Ichthyology & Herpetology*, *109*(3). https://doi.org/10.1643/i2020136

Skorczewski, T., Cheer, A., & Wainwright, P. C. (2012). The benefits of planar circular mouths on suction feeding performance. *Journal of The Royal Society Interface*, *9*(73), 1767–1773. https://doi.org/10.1098/rsif.2011.0904

Stiller, J., Short, G., Hamilton, H., Saarman, N., Longo, S., Wainwright, P., Rouse, G. W., & Simison, W. B. (2022). Phylogenomic analysis of Syngnathidae reveals novel relationships, origins of endemic diversity and variable diversification rates. *BMC Biology*, *20*(1), 75. https://doi.org/10.1186/s12915-022-01271-w

Van Wassenbergh, S., & Aerts, P. (2008). Rapid pivot feeding in pipefish: Flow effects on prey and evaluation of simple dynamic modelling via computational fluid dynamics. *Journal of The Royal Society Interface*.

Van Wassenbergh, S., Dries, B., & Herrel, A. (2014). New Insights into Muscle Function during Pivot Feeding in Seahorses. *PLOS ONE*, *9*(10), e109068. https://doi.org/10.1371/journal.pone.0109068

Van Wassenbergh, S., Strother, J. A., Flammang, B. E., Ferry-Graham, L. A., & Aerts, P. (2008). Extremely fast prey capture in pipefish is powered by elastic recoil. *Journal of The Royal Society Interface*, *5*(20), 285–296.

Whitehead, P. J. P., Bauchot, M. L., Hureau, J. C., Nielsen, J., & Tortonese, E. (1986). *Fishes of the North-eastern Atlantic and the Mediterranean*.